Outdoor-Indoor Propagation Characteristics of Peer-to-Peer System at 5.25 GHz

Yang Lu * , Jianhua Zhang * , *Member, IEEE*, Xinying Gao * , Ping Zhang * , Yufei Wu†
* Key Laboratory of Universal Wireless Communication (Beijing University of Posts and Telecommunications), Ministry of Education
†Motorola Ltd., Illinois 60196, America
Email: yanglu8215@sina.com

***Abstract*—Wideband Multiple-Input Multiple-Output (MIMO) channel measurements were preformed in outdoor-indoor scenario for peer-to-peer system at 5.25 GHz with 100 MHz bandwidth. Based on the measured data, a new power delay profile (PDP) model is proposed which is applicable regardless of the first path is the strongest or not. Time dispersion parameters and empirical model are presented. The RMS delay spread (RDS) is log-Gumbel distributed and the path number well obeys the Gao's distribution. The relationship between RDS and mean excess delay is also studied. Finally, the propagation pathways are reconstructed under the assumption of two-bounce scatterering according to the geography of the measurement site and the spatio-temporal information provided by a high resolution algorithm.**

Keywords- Channel measurement, peer-to-peer, power delay profile, time dispersion, ray tracing.

I. INTRODUCTION

The performance of a wireless communication system highly depends on the multi-path channel characteristics between transmitter (Tx) and receiver (Rx). A peer-to-peer system operates without base station and the subscribers communicate with each other directly [1]. Because of the lower antenna heights and the lower transmitted power of the users' equipments (UE), the radio channel will exhibit different propagation characteristics from the previous considered system. This can bring a new challenge to the system designer, especially for the communications occurred in outdoor-indoor scenario where the UEs are isolated by the thick building walls which have high material loss.

Channel measurement is a vital prerequisite for achieving good understanding of the radio channel, as well as for the derivation of channel models that can be used for system design and simulation. A great deal of work has been done to measure and model the Multiple-Input Multiple-Output (MIMO) channel in indoor and outdoor environments [1], [2], [3]. Nevertheless, relative less work has been carried out on the study of outdoor-indoor MIMO channel [4], [5]. Therefore, in order to make it possible to design efficient radio communication systems in the future, we performed wideband MIMO channel measurements in outdoor-indoor scenario for peer-to-peer system. Based on the measurements, the propagation characteristics of the radio channel are analyzed.

The research is funded by China National 863 Project: Wideband MIMO channel modeling and simulation in the next generation network (No.2006AA01Z258), the 111 project (No. B07005) and Motorola Ltd.

The shape of the power delay profile (PDP) directly reflects the propagation environment and gives an intuitionistic description of the power variation against delay. Previous models always consider the first arriving component as the strongest [6], thus a more accurate PDP model is needed which can be applicable whether the first arriving component is the strongest or not. Temporal parameters characterize the extent of time dispersion introduced by multi-path channels. Therefore, the distribution of RMS delay spread (RDS), path number and the relationship between RDS and the mean excess delay are also addressed. Rays' traces produce a deterministic description of the wave propagation. Based on the spatio-temporal information provided by a high resolution algorithm, we reconstruct the pathways in this scenario.

This paper is organized as follows. In Section II, the measurements setup and environment are introduced. The new PDP model and the temporal parameters are presented and analyzed in Section III. Moreover, the propagation characteristics are discussed and an attempt is made at reconstructing the pathways according to the spatio-temporal information obtained from a high resolution algorithm. Finally, conclusions are drawn in section IV.

II. DESCRIPTION OF THE MEASUREMENTS

A. Measurements Setup

The channel measurements were performed using the channel sounder Propsound [7] in Beijing, China. The measurement system parameters are summarized in Table I. Tx employs a 3D dual-polarized omni-directional array (ODA) and Rx employs a vertically polarized uniform circular array (UCA) as shown in Fig. 1 (a) and (b) respectively.

TABLE I. MEASUREMENT SYSTEM PARAMETERS

Parameter	Value
Centre frequency [GHz]	5.25
Bandwidth [MHz]	100
Tx power [dBm]	26
Tx/Rx antenna height [m]	1.5 /2.5
Tx/Rx elements	50/8
Code length [chips]	511
Chip rate [MHz]	100
Channel sampling rate [MHz]	200

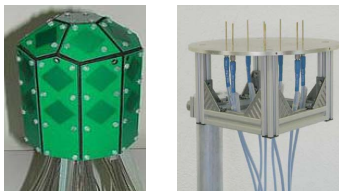

(a) (b)

Figure 1. Antenna arrays in channel measurements: (a) Tx ODA. (b) Rx UCA.

B. Environment

The measurements are performed in a building located in a typical urban environment in Beijing. Fig. 2 shows the measurements environment. Both the interior and exterior walls are made of brick and reinforced concrete. Rx is located in the corridor of the building. The floor and the sidewalls of the corridor are covered with marbles. There are also several notice boards with glass sheets along both sides of the corridor. The doors of the rooms are made of wood while the entrance doors of the building are made of glass with aluminum frame. Huge concrete poles with marble surface, escalator and some partitions made of plasterboard locate in the centre area. There are also staircase in south of Rx, behind which are cross floor windows with aluminum frame. Tx located in a few spots plotted on the street between the building and a square which contains grass, trees, a cabin and some sculptures. The street is lined with bicycles.

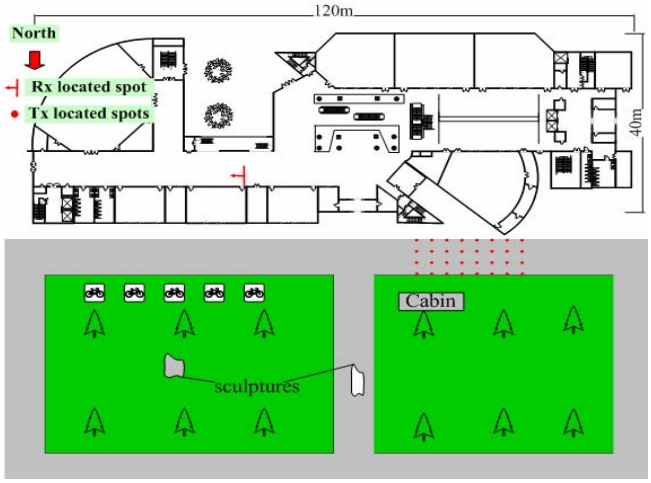

Figure 2. Layout of the measurement area.

III. Results and Analysis

A. PDP

PDP is usually simply fitted to the single-slope exponential decay function described as

$$p(\tau) = e^{-b\tau} \tag{1}$$

where τ is the excess delay in ns, b is a constant in MHz. When the latter part of the PDP has a high power caused by the paths from farther scatterers, dual-slope exponential function [6] described as:

$$p(\tau) = e^{-b_1\tau} + qe^{-b_2\tau} \tag{2}$$

is found to give better fit. However, these two equations always model the first arriving component as the strongest path. They could not reflect the real situation when the first arriving path is not the strongest component. In order to give a more accurate model which is applicable irrespective of whether the first arriving path is strongest or not, we propose a new model described as

$$P(\tau) = \frac{1-\mathrm{sgn}(\tau-c)}{2} e^{b_1(\tau-c)} + \frac{1+\mathrm{sgn}(\tau-c)}{2}[e^{-b_2(\tau-c)} + q_d e^{-b_3(\tau-c)}] \tag{3}$$

$$\text{where } \mathrm{sgn}(a) = \begin{cases} 1 & a>0 \\ 0 & a=0 \\ -1 & a<0 \end{cases} \tag{4}$$

c is the excess delay of the strongest path, b_1, b_2, b_3 and q_d are constants determined by the distribution of scatterers in the environment.

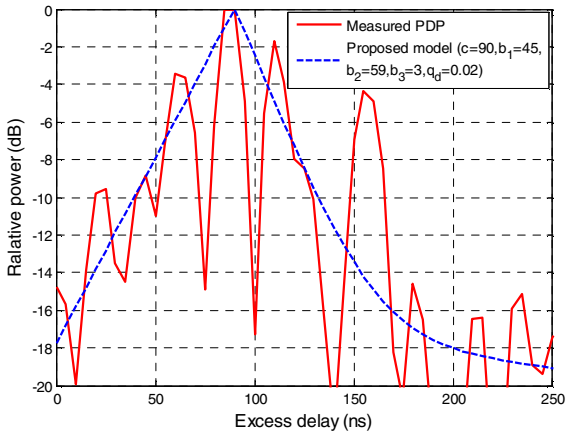

Figure 3. Typical PDP of outdoor-indoor scenario.

Fig. 3 shows a typical measured PDP fitted by the above proposed model. As we can see, the model is in reasonable agreement with the measured PDP. If the first component is the strongest, c will equal to zero and this model will change to (2) which has excellent performance in fitting the PDP as described in [6]. b_1 is affected by the distribution of the paths arrived before the strongest path. Large b_1 reflects the large power difference between the firstly arrived paths and the strongest path. This occurs in some non-line-of-sight (NLOS) case when the firstly arrived paths penetrating through walls have very low power compared with that of the strongest path arrived later by diffraction from the doorways. If the firstly arrived paths and the strongest path have similar power levels, small b_1 would be found. b_2 is affected by the scatterers located near a UE. If there are many scatterers near a UE, the PDP behind the strongest path will decay slowly and smaller b_2 would be found. Otherwise, this part will decay quickly and larger b_2 would be found. b_3 is similar with b_2 but affected by the scatterers located in the longer distance and influence the tail of the PDP. q_d is determined by the ratio of the number of farther scatterers to that of near scatterers. The more scatterers

located in farther distance, the larger q_d will be and vice versa. The typical values of c, b_1, b_2, b_3 and q_d in our outdoor-indoor measurements are 80 to 110 ns, 30 to 50 MHz, 45 to 75 MHz, 1 to 15 MHz and 0.01 to 0.15 respectively.

B. Delay Parameters

Time dispersion parameters shed some light on the temporal distribution of power relative to the first arriving components. They are obtained by using the PDPs derived from the measured channel impulse responses (CIRs). A threshold is set to remove the noise contribution. In this paper, we use dynamic threshold which equals to noise floor plus 10dB and only the PDPs with dynamic range larger than 25dB are considered as valid samples. The noisefloor is calculated from the part of the PDP in which no signal components arrived.

Table II summarizes the 10%, 50% and 90 %, mean, standard deviation values of the cumulative distribution functions (CDF) of the selected delay parameters.

TABLE II.

PERCENTILES OF RDS, MAXIMUM AND MEAN EXCESS DELAY

	RDS (ns)	Max excess delay (ns)	Mean excess delay (ns)
10%	24.5	120.0	44.0
50%	36.5	200.0	66.5
90%	48.0	280.0	87.0
mean	36.4	200.2	66.1
std	9.2	60.1	16.9

Examining the distributions of the small scale parameters can be helpful in better understanding the characteristics of the channel. The measured RDS probability density function (PDF) is fitted with the following theoretic distributions to find out the best fit:

1) Normal distribution (PDF)

$$f(x)=\frac{1}{\sqrt{2\pi}\sigma}e^{-\frac{(x-\mu)^2}{2\sigma^2}} \tag{5}$$

2) Logistic distribution (PDF)

$$f(x)=\frac{e^{\frac{x-\mu}{\sigma}}}{\sigma(1+e^{\frac{x-\mu}{\sigma}})^2} \tag{6}$$

3) Gumbel distribution (PDF)

$$f(x)=\frac{1}{\sigma}e^{\left(-\frac{x-\mu}{\sigma}-e^{\frac{x-\mu}{\sigma}}\right)} \tag{7}$$

where μ and σ are the mean and standard deviation of the distribution respectively. Compared with Normal distribution, the left-skewed Gumbel distribution has higher probability in smaller values. Therefore, it is particularly convenient for small extreme values. Logistic distribution is similar with Normal distribution in shape but it has longer tails. Normal distribution is most centralized to the mean value in the three distributions.

Mostly, Log-normal distribution is found to provide the best fit to the measured RDS distribution [2]. However, in outdoor-indoor scenario, the pathways are more confined than in other scenarios. Paths mainly travel through wall openings, i.e. doorways and windows [8]. When Tx locates at some spots, certain paths penetrated through walls or undergone longer distances can not be detected due to the lower transmitted power and the penetration loss of the walls. Only the paths propagated from windows and doorways are obtainable. This increases the number of smaller RDS values and makes the empirical data's PDF left-skewed. As a consequence, as Fig. 4 shows, fitting the log of the measured RDS with different distributions defined by (5) (6) (7), Gumbel distribution gives the best fit with the minimum rmse of 0.076. Such highly confine to the path propagation is a specific situation owned by outdoor-indoor scenario since the penetration loss of the exterior wall of the building is usually dramatically high. In other scenario when this confine does not exist, the propagation traces will be more diversiform and log-normal or log-logistic distributed RDS would be found.

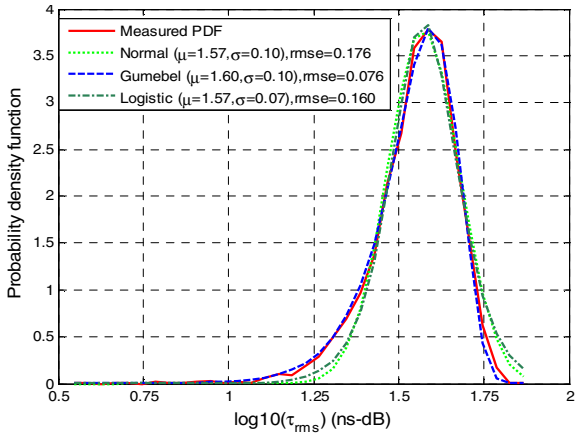

Figure 4. Distributions of the RDS.

The path number distribution is commonly fitted by Poisson distribution which can be expressed as

$$P(N)=\frac{\eta^N\cdot e^{-\eta}}{N!} \tag{8}$$

where N and η are the variable denoting the path number and the mean path number. In [9], Gao's distribution is considered to have better fit than Poisson distribution especially at high probability values. It can be described as

$$P(N)=C_{N_T}^{N}\frac{\eta^{N_T-N}}{(1+\eta)^{N_T}} \tag{9}$$

where N is a variable representing the path number, C means combination, and N_T is the maximum path number that can be received. The mean path number is $N_T/(1+\eta)$.

For comparative purposes, Fig. 5 shows the path number distribution fitted by Poisson and Gao's distribution. As we can see, Gao's distribution is more centralized to the mean value while Poisson distribution has longer tails. As mentioned above, since the pathways are highly confined, the probability of rays' barging up against objects which may cause reflection, diffraction, and scattering decreases. As a result, the path number distribution is more centralized to the mean value. Therefore, the path number distribution is in better agreement with Gao's distribution than Poisson distribution.

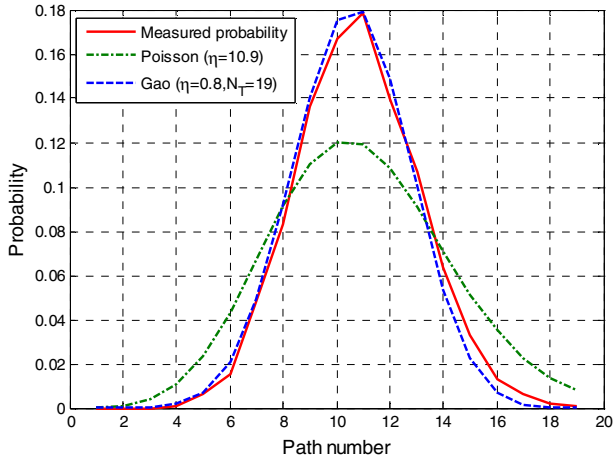

Figure 5. Path number distribution.

C. RDS and Mean Excess Delay

The dependence of the RDS on mean excess delay has been analyzed based on the measurements. Generally, the linear relationship between RDS and mean excess delay is in the form [10]

$$\tau_{rms} = a \cdot \tau_{mean} + b \tag{10}$$

where a is the RDS variation factor against the mean excess delay which indicates the density of the scatterers per unit distance in the environment. If Tx and Rx locate in an environment containing richer scatterers, such as typical urban area, increasing the Tx-Rx separation could include more scatterers participated in the paths' propagation. Thus RDS increases markedly with the mean excess delay and this is reflected by large value of a. If the environment contains few scatterers, such as some open area in rural region, the increase of the Tx-Rx separation would not make the RDS increase much and small value of a would be found.

The relationship can also serve as a measure of the time dispersion characteristics of the environment [11]. If the multi-path PDP decays exponentially over the time delay, $\tau_{rms} = \tau_{mean}$ would be found. The case that the PDP has a high concentration of power at small excess delay is reflected by $\tau_{rms} > \tau_{mean}$. This results from the situation that the PDP is dominated by the first a few strong components arriving at early time which heavily influence τ_{mean}, while there are some weaker components in the very late time influenced τ_{rms} highly. $\tau_{rms} < \tau_{mean}$ demonstrates the situation that the main energy arrived at the mid point but not the early part of the PDP.

In our measurement, the firstly arrived paths correspond to the ones traveling directly towards the windows, doorways and reach Rx by penetrating through the interior walls. While the group of paths arrived at longer delay contains not only the ones propagated via the objects in the centre of the hall and corridor, but also the ones reflected by the cabin opposite Tx. Thus the middle part of the PDP contains more energy and larger mean excess delay is obtained compared with RDS. Fig. 6 shows the measured data and the fitted line with a, b equal to 0.52 and 0.59 respectively. The solid line is the referenced line for mean excess delay equals to RDS. It is apparent to see, RDS is smaller than mean excess delay in almost all the points.

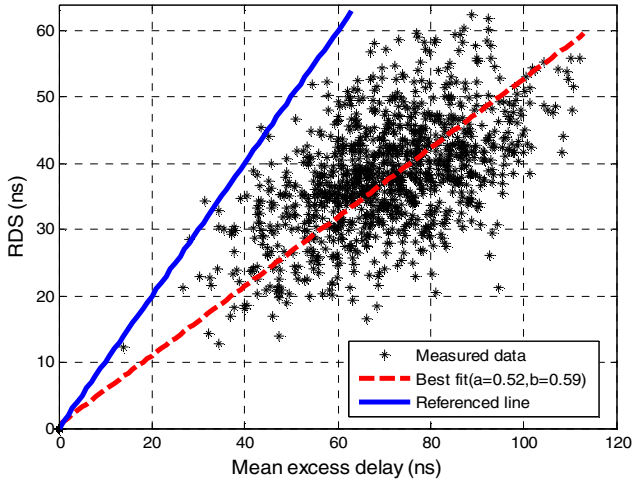

Figure 6. RDS vs mean excess delay.

D. Discussion of the Pathways Based on SAGE Results

In order to evaluate the propagation characteristics in more details, SAGE (Spatial-Alternating Generalized Expectation-maximization) algorithm [12] is applied to the measurement data which can provide detail information of each path, such as the complex weight, delay, angle of arrival (AOA) and angle of departure (AOD). Fig. 7 shows one snapshot of the 34 multi-path components (MPCs) estimated by SAGE.

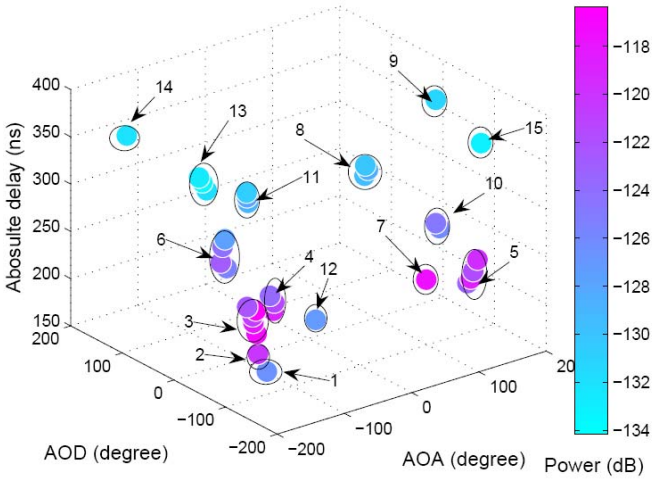

Figure 7. MPCs of a typical measurement spot..

Since these parameter estimates of each path are automatically associated and the locations of Tx and Rx are always known, it is possible to infer the likely propagation pathways of most estimated paths by using the ray tracing techniques described in [13]. No one-bounce path could be inferred due to the complexity of the measurement environment and we reconstruct the propagation pathways under the assumption that propagation occurs via two bounce scatterering. A two-bounce path is identified if its distance is consistent with the estimated propagation delay within an uncertainty of 1 ns. For simplicity, we firstly assign these MPCs into 15 clusters by visual inspection. The MPCs

belonging to the same cluster should have similar AOA, AOD, and delay. Then, we reconstruct these clusters propagation traces according to the mean AOA, AOD and delay of the MPCs belonging to each cluster.

The reconstructed propagation traces are shown in Fig. 8. 10 out of 15 clusters' propagation traces are identified. Cluster 1, 2, 3, 4, 5, 7, 10, and 12 propagate via windows. Cluster 1, 3, 12 penetrate through one layer of the wall while cluster 2, 4, 5, 7, 10 propagate via doors of the rooms. Cluster 6 is reflected by the cabin and propagates through doorways of the building. Cluster 8 also propagates through doorways, but penetrates two layers of the walls and then is reflected by the east end of the corridor. Cluster 9 and 13 could not be related to the environment since the centre of the corridor contains richer scatterers. Cluster 11, 15 also could not be identified. They are supposed to undergo more bounce interactions in the corridor and the last bounce is related to the scatterers around spot 'A' denoted in Fig. 8 according to their AOAs. Cluster 14 is supposed to interact on the surface of the building by considering its AOD and the most likely propagation way is that the wave is firstly reflected by the surface of the building and then collides on the cabin, travels through doorways by diffraction. Propagation paths with more than two bounces could be identified that are consistent with the estimated parameters of these clusters but more sophisticated validation procedures are needed to infer the wave interactions with more than two objects.

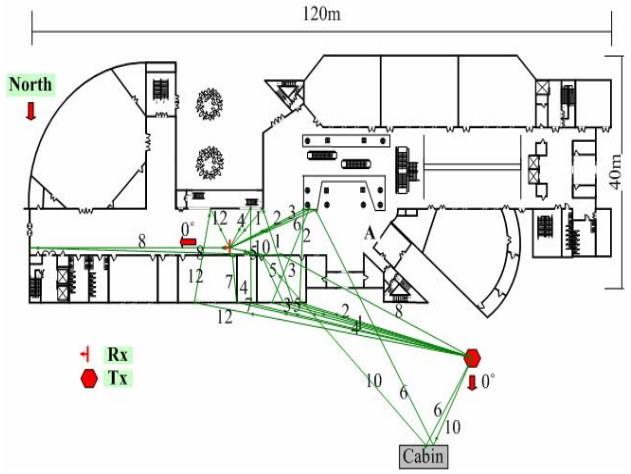

Figure 8. Reconstructed two-bounce propagation paths.

From Fig. 8 we can conclude that in outdoor-indoor scenario, paths mainly travel through wall openings, such as windows and doorways .Windows introduce little penetration loss to the paths. Few paths can penetrate through two layers of the walls because of the high penetration loss of the wall and the low transmitted power of the UEs in the peer-to-peer system. Only the paths propagated via the near scatterers are obtainable. Paths coming from the far scatterers such as trees and sculptures located in the square opposite the building could not be detected due to the high path loss introduced by the long travel distance.

IV. CONCLUSION

In this paper a new PDP model is proposed which is applicable in despite of whether the first arriving path is the strongest or not. It is shown that the model is in good agreement with the measured PDP. Time dispersion parameters are studied and modeled based on the measurement. The RDS is found to be log-Gumbel distributed and the path number well obeys the Gao's distribution. The relationship between RDS and mean excess delay is also studied. Based on the spatio-temporal information provided by SAGE, the propagation pathways are reconstructed according to the geography of the measurements environment and some conclusions about the propagation characteristics in outdoor-indoor scenario are drawn. These results can be used in the future study of the outdoor-indoor propagation characteristic of peer-to-peer system.

ACKNOWLEDGMENT

The authors would like to thank the engineers of Elektrobit Company, Finland for their efforts in our measurement campaign. Useful help and discussions from Jukka-Pekka Nuutinen are greatly appreciated.

REFERENCES

[1] N. Patwari, G. D. Durgin, T. S. Rappaport, R. J. Boyle, "Peer-to-peer low antenna outdoor radio wave propagation at 1.8 GHz,"IEEE VTC, 49th. vol. 1, pp. 371 - 375, Jul. 1999.

[2] IST-2003-507581, WINNER, "Final report on link level and system level channel models," D5.4 ver 1.4, Nov. 2005.

[3] X. Zhao, J. Kivinen and P. Vainikainen, "Propagation characteristics for wideband outdoor mobile communications at 5.3GHz," IEEE Journal on selected areas in communications, vol. 20, no. 3, pp. 507 - 514, Apr. 2002.

[4] A. M. Street and A. P. Jenkins, "Outdoor-indoor radio channel propagation study," Tech. Rep.OXOSPC-REP1, Communications Group, Dept. of Eng. Science, University of Oxford, Nov. 1998.

[5] S. Wyne, P. Almers, G. Eriksson, et. "Outdoor to indoor office MIMO measurements at 5.2GHz", VTC , vol. 1, pp. 101 – 105, Sept. 2004.

[6] T. Zwick, C. Fischer, W. Wiesheck, "A stochastic multipath channel model including path directions for indoor environments," IEEE Journal on selected areas in communications, vol. 20, no. 6, pp. 1178 - 1 192, Aug.2002.

[7] A. Stucki et. al., "PropSound system specifications document: concept and specifications," Elektrobit AG, Switzerland, Internal Report, 2001.

[8] Y. Miura, Y. Oda and T. Taga, "Outdoor-to-indoor propagation modeling with the identification of path passing through wall openings," Proc. of 13th IEEE International Symposium on Personal, Indoor and Mobile Radio Communications (PIMRC 2002), Lisboa, Portugal, vol. 1, pp. 130 – 134, Sept. 2002.

[9] S. Gao, S. Zhong, and C. Jiang, "Path number distribution for multipath propagation in land mobile communications and its simulation" (in Chinese), J. China Inst. Commun., vol. 19, no. 2, pp. 66 -72, Feb. 1998.

[10] M. S. Varela, M. G. Sanchez, "RMS delay and coherence bandwidth measurements in indoor radio channels in the UHF band," .IEEE Transactions on Vehicular Technology, vol. 50, no. 2, pp. 515 - 525, Mar. 2001.

[11] T. S. Rappaport, "Characterization of UHF multipath radio channels in factory buildings," Antennas and Propagation, IEEE Transactions on vol. 37, no. 8, pp. 1058 - 1069, Aug. 1989.

[12] B. H. Fleury, M. Tschudin, R. Heddergott, D. Dahlhaus, and K. I. Pedersen, "Channel parameter estimation in mobile radio environments using the SAGE algorithm," IEEE Journal on selected areas in communications, vol. 17, no. 3, pp. 434 – 450, Mar. 1999.

[13] B. H. Fleury, X. Yin, K. G. Rohbrandt, P. Jourdan and A. Stucki, "High-resolution bidirection estimation based on the SAGE algorithm: Experience gathered from field experiments," TD02 (70), COST 273, Espoo, Finland, May. 2002.